Agricultural Water Management 310 (2025) 109367

Contents lists available at ScienceDirect

Agricultural Water Management

journal homepage: www.elsevier.com/locate/agwat

Time-frequency insights: Uncovering the drivers of reference evapotranspiration across China

Shuting Zhao[a,1], Jinglong Wu[a,1], Rangjian Qiu[a,*], Tao Zhang[a], Yufeng Luo[a], Wei Hu[b]

[a] State Key Laboratory of Water Resources Engineering and Management, School of Water Resources and Hydropower Engineering, Wuhan University, Wuhan 430072, China

[b] The New Zealand Institute for Plant & Food Research Limited, Private Bag 4704, Christchurch 8140, New Zealand

ARTICLE INFO

Handling Editor - Dr. Brent Clothier

Keywords:
Multiple-wavelet coherence
Percentage area of significant coherence
Phase angle
Wavelet transform coherence

ABSTRACT

Reference evapotranspiration (ET_o) is an important variable required in many disciplines and is influenced by many factors. However, the bivariate and multivariate relationships between ET_o and affecting factors across multiple time-frequency domains remain unknown. Here, we identified the primary factors affecting ET_o across time-frequency domain in 653 meteorological stations of mainland China based on the combination of wavelet transform coherence (WTC) and multiwavelet coherence (MWC) methods. The results indicated that ET_o and all affecting factors (solar radiation, R_s; vapor pressure deficit, VPD; air temperature, T_a; wind speed, u_2) during 1967–2016 exhibited a frequency ranging from 2 days to 211 months, and had a continuous annual (374 d) periodicity (except u_2) for almost all sites. Results of percentage area of significant coherence (PASC) of WTC indicated that VPD or R_s is the dominant single factor driving variations of ET_o across time-frequency space in majority sites (66.3 % and 32.0 %, respectively), while u_2 is only dominant in limited (11) sites. This quite differs from the daily scale, where daily ET_o was primarily influenced by daily R_s at 361 sites, daily VPD at 286 sites, and daily T_a at 6 sites. Results of MWC showed that the explanation for the time-frequency variations of ET_o can be further improved using two-factors in 40.7 % of all sites as indicated by absolute increased PASC of MWC by 5 %. Overall, we found that the variation of ET_o across time-frequency domain can be well explained by using only one variable (VPD or R_s) in 59.3 % of all sites, while by combinations of VPD-R_s and VPD-u_2 in remaining sites. This study provides novel insights into understanding the variations of ET_o across multiple time-frequency spaces.

1. Introduction

The reference evapotranspiration (ET_o), representing the atmospheric evaporation demand at a specific location, is a crucial variable for computing crop and vegetation evapotranspiration through the two-step crop coefficient-ET_o method (Allen et al., 1998; Pereira et al., 2015; Qiu et al., 2025). Additionally, the ET_o is a critical variable for characterizing local climate by defining the aridity index ($AI = P / ET_o$, P is the mean annual precipitation) (Hu et al., 2021; Pour et al., 2020; Qiu et al., 2022; Xiang et al., 2020). Hence, information of ET_o is frequently needed in agriculture, hydrology, meteorology, climatology, ecology, and environmental science, geophysics, among others (Fan et al., 2018; Li et al., 2012; Paredes and Pereira, 2019).

The comprehensive FAO56 Penman-Monteith equation is a standardized method for calculating ET_o, which adopts a set of meteorological data and incorporates the principle of soil-vegetation interaction (Allen et al., 1998). This Penman-Monteith ET_o represents the evapotranspiration from a specified reference grass/alfalfa surface and can be computed using only meteorological data (Allen et al., 1998). The Penman-Monteith ET_o is widely applied worldwide (Paredes et al., 2021; Pereira et al., 2015; Qiu et al., 2015, 2022; Rallo et al., 2021), as indicated by that FAO 56 has been cited by over 30,000 citations, where majority users utilized the Penman-Monteith ET_o (Pereira et al., 2021). The calculation of the Penman-Monteith ET_o needs full meteorological data, including solar radiation (R_s), air temperature (T_a), relative humidity (RH) or vapor pressure deficit (VPD, calculated using T_a and RH), and wind speed at 2 m height (u_2). Therefore, the variability of ET_o is affected by these aforementioned meteorological factors and differs

* Corresponding author.
E-mail address: qiurangjian@whu.edu.cn (R. Qiu).

[1] Both authors contributed equally to this manuscript.

https://doi.org/10.1016/j.agwat.2025.109367
Received 9 December 2024; Received in revised form 7 February 2025; Accepted 9 February 2025

regionally (Liu et al., 2024; Zhao et al., 2024). For instance, the most sensitive meteorological variable to ET_o is RH in the Loess Plateau region, China (Li et al., 2017), and is R_s in the West Liao River basin, China (Gao et al., 2017). In peninsular Malaysia, minimum air temperature (T_{min}) is the most influencing factor of ET_o variabilities (Pour et al., 2020). In the Siberian River Basin of the Arctic, VPD and u_2 are the primary drivers of ET_o variabilities at most stations, while T_a and R_s have relatively minor contributions (Tang and Tang, 2021). Other studies showed that R_s and VPD were the primary drivers influencing ET_o in California, USA (Ahmadi et al., 2022), while T_a and RH had the most significant impact on ET_o at 18 sites in Iran (Valipour et al., 2017). These above results showed that there are high variabilities of ET_o in response to primary meteorological drivers at varying regions. Therefore, a better understanding of the regulation and primary drivers of ET_o across varying regions is critical to explore the evolution of ET_o and is indispensable for developing accurate estimation and forecasting methods for ET_o (Nourani et al., 2019).

It is noteworthy that the nature and importance of ET_o shows significant differences at different time scales, for instance, understanding the immediate water demand of crops at the daily scale (Pereira and Pruitt, 2004); developing effective irrigation schedules over several days, monthly or seasonal scale (Citakoglu et al., 2014); and assessing the impact of climate change on agricultural production at the annual scale (Shi et al., 2017). Therefore, an in-depth investigation of the properties and roles of ET_o at different time scales is important for agricultural water management and climate adaptation research (Tie et al., 2018). To identify the key meteorological factors influencing daily, monthly, or annual ET_o, many scholars have employed a variety of methods, including multiple linear or stepwise regression analysis (Gao et al., 2017; Wang et al., 2017), (partial) correlation analysis (Han et al., 2018), principal component analysis (Zarei et al., 2021), path analysis (Wang et al., 2023) and machine learning algorithms (e.g. K-nearest neighbor (Zhao et al., 2022) and random forest (Ahmadi et al., 2022)), among others. In addition, some studies developed a comprehensive method to determine the contribution of a factor to ET_o by multiplying the sensitivity coefficient of a single factor by its relative change rate (Li et al., 2017; Yang et al., 2019).

Until now, majority studies concerned the variation of ET_o at a specific time-scale, such as daily, monthly, or annual scale (Khanmohammadi et al., 2017; Liang et al., 2010), aiming to explore the patterns and trends of ET_o evolution over time and the relation between ET_o and affecting factors at a specific time scale (Liu et al., 2024). However, the ET_o and its key affecting factors are varied spanning multiple time scales. For instance, on daily scale, R_s is the most important meteorological factors affecting ET_o in China, followed by T_a (Zhao et al., 2022). At the monthly scale, u_2 is the most important factor affecting ET_o in China and Iran, followed by T_{max}, R_s, and RH (Khanmohammadi et al., 2017; Wang et al., 2017). At the annual scale, T_a, RH, and R_s are the major factors in Bangladesh (Jerin et al., 2021). However, the variability of ET_o and its primary driving force across multiple time-frequency domains is seldom explored.

Wavelet transform methods are commonly utilized to detect dominant periodicities (Araghi et al., 2015; Joshi et al., 2016) and multi-scale correlations between time series (Chou, 2011; Wu et al., 2019). Among them, the widely used continuous wavelet transform method (CWT) can not only provide high-resolution analyses within the temporal domain and capture the dynamic characteristics of time series across different temporal scales, but also elucidate the variability among distinct geographic regions (Martínez and Gilabert, 2009; Rhif et al., 2019). At the time scale, CWT elucidates the variation and periodic characteristics of variables across diverse temporal scales (from seconds to years) (Hu and Si, 2021), and decomposes the data into a series of sub-signals with varying frequencies for discerning their trends and correlations (Sang, 2013). At the spatial scale, CWT can be used to evaluate the variability in the spatial distribution of variables and their affecting factors, thereby determining the degree to which this variability impacts the variables (Joshi et al., 2016).

The CWT can also be used to determine wavelet transform coherence (WTC), which is a correlation coefficient in the time-frequency domain used to quantitively evaluate the degree of linear correlation between two nonstationary series in the time-frequency space (Cazelles et al., 2008). The CWT and WTC have been widely used to investigate the spectral characteristics and single primary affecting factor of many response variables (Ding et al., 2013; Jerin et al., 2021; Sreedevi et al., 2022; Sun et al., 2020; Zhou et al., 2022), such as daily streamflow (Tao et al., 2024), air pollutant concentration (Kim et al., 2021), groundwater level (Wu et al., 2021), crop evapotranspiration (Ding et al., 2013; Zhang et al., 2023), and pan evaporation (Ghaemi et al., 2019), but not for ET_o yet.

Moreover, the variability of many response variables, such as ET_o, is affected by multiple factors. Therefore, it is necessary to adopt multivariate methods to capture the coherence between dependent variables and multivariate. Since the traditional multivariate methods cannot identify localized information at a specific scale and neglect the correlation between factor variables, these methods may identify redundant factor variables, therefore are not the most effective way to explain the variation of the dependent variables (Hu et al., 2017). Recently, a multiple wavelet coherence method (MWC) has been proposed (Hu and Si, 2016), which can capture the multivariate correlations at varying time scales, and determine the proportion of the dependent variance explained by factor variables at multiple time-frequency space (Hu and Si, 2016; Wu et al., 2023). The MWC have been also applied to explore the correlation between large rivers of world, soil water content, evaporation and their multivariate (Hu et al., 2017; Hu and Si, 2016; Su et al., 2019), but have not been adopted for ET_o yet.

The variability of ET_o is affected by various meteorological factors and has varying dominant factors at multiple time scales as aforementioned, and the relationship between ET_o and these factors remains unknown at multiple time-frequency domains (Mahmoud and Gan, 2020). ET_o and its influencing factors are often time-varying and non-stationary (Kang et al., 2022). Simple time- or frequency-domain analyses are unable to capture these variations comprehensively, whereas time-frequency analyses are able to capture these transient features and reveal the hidden patterns and characteristics of these complex relationships (Ding et al., 2019), thus providing a more comprehensive understanding of the dynamic behaviors and trends of ET_o.

Compared to a single time scale, time-frequency analysis provides information about ET_o and its influencing factors in both time and frequency dimensions, and has a comprehensive view to understand the ET_o changes. In addition, the time-frequency analysis is able to decompose the signal and reveal its characteristics at different time scales (Feng et al., 2013). This enables researchers to more accurately locate and analyze the transient features of ET_o, such as mutation point (Luo and Xiao, 2014), periodicity (Chong et al., 2019) and trend (Jerin et al., 2021).

However, the meteorological factors affecting ET_o at multiple time-frequency domains have been rare explored at present. In addition, majority studies have concerned variability of ET_o and its affecting factors on a specific time scale at individual site or small regions (Gocić et al., 2015; Liang et al., 2010), which constrains a comprehensive understanding of large temporal-spatial scale processes and their spatial heterogeneity.

Therefore, we employed the wavelet transform method to analyze the correlations between ET_o and varying meteorological factors across multiple time-frequency domain from 653 stations across mainland China. The objectives of this study were: (1) to detect temporal patterns of the ET_o and affecting meteorological factors using CWT; (2) to analyze the relations between ET_o and single meteorological factor across multiple time-frequency domains in mainland China by using the WTC; (3) to determine whether combinations of two factors at each site selected based on WTC can further increase the explanation of ET_o across multiple time-frequency space by using MWC.

2. Data and methods

2.1. Data collection

In this study, we collected continuously daily meteorological data including maximum and minimum temperature (T_{max} and T_{min}, °C), mean RH (RH_{mean}, %), sunshine duration (n, h), and wind speed at a height of 10 m (u_{10}, m s^{-1}) from the China Meteorological Data Service Centre (CMA Meteorological Data Centre, 2019). These strictly quality–controlled daily data were collected from 653 meteorological stations across mainland China covering the period 1967–2016. The criterion of surface meteorological observation was employed to control the quality of all aforementioned measured data. Based on data description documents, the accuracy of these collected data after data quality control is ~100 %. The missing data was less than 0.5 % for all variables, and less than 1.5 % for individual variables for each site (we have collected the data from 805 stations, while 653 stations meet this criterion). Since the rarity of continuous missing data, all data at a given day were excluded if any of the above variables were absent.

We selected VPD, R_s, T_a, and u_2 as the key factors for assessing the influence of ET_o based on the significance of variables on ET_o across multiple time-frequency space. VPD and R_s are universally acknowledged as primary determinants of ET_o. Specifically, VPD, a metric of atmospheric aridity, serves as a critical impetus for water evaporation (Zhou et al., 2019); R_s, a fundamental component of the surface energy balance, exerts a direct influence on both surface temperature and evaporation rates (Ahmadi et al., 2022).

Furthermore, T_a influences ET_o indirectly by modulating the atmospheric capacity to retain water vapor and the surface energy balance (Qiu et al., 2019), and u_2 regulates evaporation process by influencing airflow dynamics and boundary layer characteristics (Ahmadi et al., 2022). While they may not always dominate, they often contribute additional insights in multivariate modeling frameworks, thereby augmenting the explanatory capacity of models. Other factors, such as net radiation (R_n), though correlated with ET_o, exhibit a strong correlation with R_s, potentially giving rise to multicollinearity issues.

The variation of ET_o is closely related to climatic regions. To reveal the spatial distribution pattern of coherence between ET_o and meteorological factors, we divided mainland China into seven climatic zones based on the characteristics of the typical vegetation (Yao et al., 2018; Zhao et al., 1983) (Fig. 1), i.e. mid-temperate arid region (I), mid-temperate semi-arid region (II), mid-temperate semi-humid region (III), warm temperate semi-humid region (IV), northern subtropical humid region (V), marginal tropical humid region (VI), and plateau temperate semi-arid region (VII).

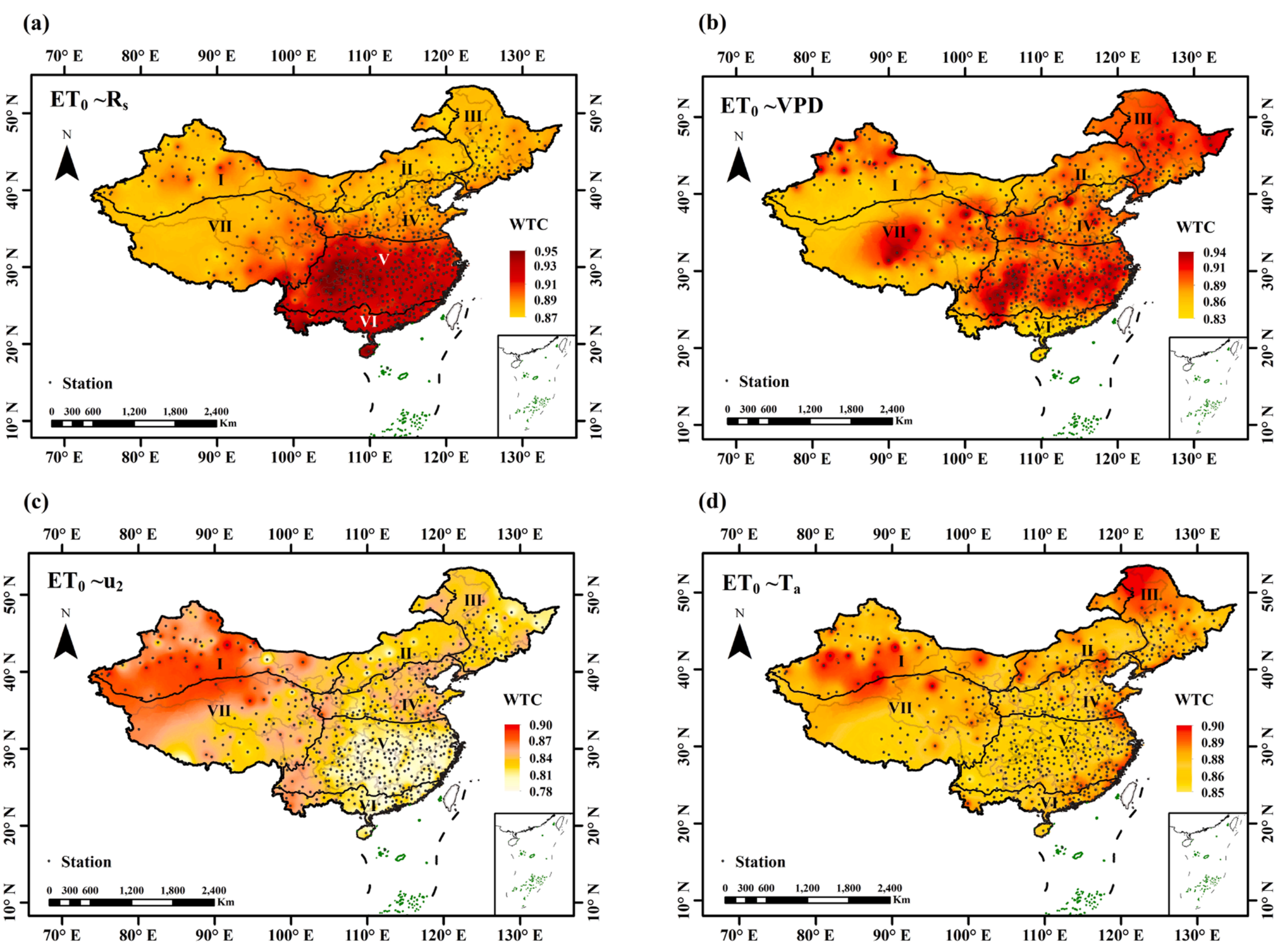

Fig. 1. Spatial distribution of significant wavelet transform coherence (WTC) values between the reference evapotranspiration (ET_o) and solar radiation (R_s; a), vapor pressure deficit (VPD; b), wind speed at 2.0 m height (u_2; c), and air temperature (T_a; d) across time-frequency domain. I-VII are mid-temperate arid region, mid-temperate semi-arid region, mid-temperate semi-humid region, warm temperate semi-humid region, northern subtropical humid region, marginal tropical humid region, and plateau temperate semi-arid region, respectively.

2.2. The calculation of ET_o

The FAO 56 Penman-Monteith equation to determine daily ET_o (mm d^{-1}) is as follows (Allen et al., 1998)

$$ET_o = \frac{0.408\Delta R_n + \gamma \frac{900}{T_a+273} u_2 VPD}{\Delta + \gamma(1+0.34u_2)} \tag{1}$$

where T_a is the daily mean air temperature (°C; $=(T_{max}+T_{min})/2$); Δ and γ are the slope of the vapor pressure curve (kPa °C^{-1}) and the psychrometric constant (kPa °C^{-1}); u_2 is the wind speed at a height of 2 m (m s^{-1}), can be converted from u_{10}; VPD is the daily vapor pressure deficit (kPa), which can be calculated from measured T_{max}, T_{min}, and RH_{mean} as follows (Paredes and Pereira, 2019)

$$e_a = \frac{RH_{mean}}{50\Big/\left(0.6108e^{\frac{17.27T_{max}}{T_{max}+237.3}}\right) + 50\Big/\left(0.6108e^{\frac{17.27T_{min}}{T_{min}+237.3}}\right)} \tag{2}$$

$$VPD = e_s - e_a \tag{3}$$

where e_s is the saturated vapor pressure (kPa); e_a is the actual vapor pressure (kPa). R_n is the daily net radiation (MJ m^{-2} d^{-1}), and can be calculated from daily R_s (MJ m^{-2} d^{-1}). The R_s can be calculated based on measured n, as (Allen et al., 1998)

$$R_s = \left(a_s + b_s\frac{n}{N}\right)R_a \tag{4}$$

where a_s (0.25) and b_s (0.50) are the regression constants; n is the measured sunshine duration (h); N is the maximum possible sunshine duration (h); R_a is the extraterrestrial radiation (MJ m^{-2} d^{-1}).

The R_n can be calculated as (Allen et al., 1998)

$$R_n = R_{ns} - R_{nl} \tag{5}$$

$$R_{ns} = (1-\alpha)R_s \tag{6}$$

where R_n is the net radiation (MJ m^{-2} d^{-1}); R_{ns} is the net solar radiation (MJ m^{-2} d^{-1}); α is the albedo (0.23 for grass); R_{nl} is the net longwave radiation (MJ m^{-2} d^{-1}), which is obtained from temperature by using Stefan-Boltzmann equation. The detailed calculation formulas of N and R_a as well as Δ, γ and u_2 are described elsewhere (Allen et al., 1998).

2.3. Wavelet method

In this study, we first revealed the temporal patterns of ET_o as well as meteorological factors (R_s, T_a, VPD, and u_2) by using continuous wavelet transform (CWT) method. Next, the bivariate coherence and multiple-wavelet coherence among ET_o and affecting factors were calculated by using WTC and MWC.

2.3.1. CWT

The CWT utilizes wavelet functions that are well-localized in both time and frequency (Gedalof et al., 2004). This dual localization enables the CWT to offer detailed insights into the characteristics of signal within the time-frequency domain (Grinsted et al., 2004). For a wavelet function $\Phi(t)$, after selecting a center frequency, transforming it using the scale factor s can then obtained a large set of center frequencies. Additionally, a series of basis functions with varying intervals can be obtained through the translation factor u by translating on a temporal scale. The inner product operation is performed with a segment of the original signal (the signal of time series for the ET_o) respectively, obtaining the extreme value which corresponds to the frequency contained in this interval of the original signal.

Therefore, for the time series x_i ($i = 1, 2, \ldots, n$) with sample length n and equal sample intervals Δt, the inner product of the original time-domain signal and the wavelet function reflects the component size of the signal in the direction of the wavelet function. When the wavelet functions are in the time-frequency translation, expansion, and contraction, the wavelet functions can be gained with varying center frequencies and positions. The CWT can be considerate as the convolution process of the time-domain signal with a specific wavelet function $\Phi\left(\frac{t-u}{s}\right)$ as the convolution window, as (Maraun and Kurths, 2004)

$$W_u{}^X(s) = \sum_{i=1}^{n} x_i \Phi_0^*\left(\frac{t_i-u}{s}\right) \tag{7}$$

$$\Phi\left(\frac{t_i-u}{s}\right) = N(s)\Phi_0\left(\frac{t_i-u}{s}\right) \tag{8}$$

where $W_u{}^X(s)$is the value of CWT with a translation factor of $u = j\Delta t$ and a scale factor of s; $N(s) = \sqrt{\frac{\Delta t}{s}}$ is the normalization factor that makes the wavelet energy unitary, and detailed calculation is shown elsewhere (Grinsted et al., 2004); * indicate complex conjugation.

In this study, we chosen the zero-mean Morlet-wavelet, which is easy to obtain information of the instantaneous frequency and phase of the signal because its real part is 90° phase-shifted from the imaginary part and has good resolution in the time-frequency domain (Grinsted et al., 2004; Torrence and Compo, 1998) and can be calculated as (Grinsted et al., 2004)

$$\Psi_0(t) = \pi^{-1/4} e^{i\omega_0 t} e^{-t^2/2} \tag{9}$$

where ω_0 is dimensionless frequency and t is dimensionless time.

2.3.2. Wavelet Transform Coherence (WTC)

The WTC is a method used to quantitatively analyze the degree of association between two nonstationary time series in a time-frequency space, i.e. it is similar to correlation coefficient in time-frequency space (Cazelles et al., 2008). The WTC is particularly useful for identifying periods and locations where two-time series are correlated and the degree of this correlation. The expected performance for WTC depends on the cost of reducing the magnitude of localized time-frequency domain (Grinsted et al., 2004). For time series X and Y, after using wavelet transforms $W_u^X(s)$ and $W_u^Y(s)$, wavelet coherence, R_u^2 [0,1], can be defined as (Torrence and Compo, 1998)

$$R_u^2(s) = \frac{\left|S\left(s^{-1}W_u{}^{XY}(s)\right)\right|^2}{S\left(s^{-1}\left|W_u{}^X(s)\right|^2\right)S\left(s^{-1}\left|W_u{}^Y(s)\right|^2\right)} \tag{10}$$

where S is the smoothing operator defined by the type of wavelet used; u is the position time index and:

$$S(W) = S_{scale}(S_{time}(W_u(s))) \tag{11}$$

$$W_u{}^{XY}(s) \equiv W_u{}^X(s) W_u{}^{Y*}(s) \tag{12}$$

where S_{scale} and S_{time} are corresponding smoothing along the wavelet scale axis and in time, which are designed to have a similar footprint as the adopted wavelet (Torrence and Compo, 1998). More detailed description and computation of WTC are shown elsewhere (Grinsted et al., 2004).

In addition, the wavelet phase between Y and an independent variable (X_1) can be calculated as

$$\varphi\left(s,u\right) = \tan^{-1}\left(\frac{I_m(w^{Y,X_1}(s,u))}{R_e w^{Y,X_1}(s,u)}\right) \tag{13}$$

where I_m and R_e are the corresponding imaginary and real parts of $w^{Y,X_1}(s,u)$. It is noteworthy that wavelet phase between Y and X_1 are unavailable by using MWC. The results of the phase angle calculations help to further understand the relative relationship between ET_o and primary affecting meteorological factors in terms of temporal variations. The phase angle greater (or lower) than zero shows that the variation of

ET_o is lagging behind (or ahead) of a meteorological factor on a certain period.

The frequencies between the ET_o and four individual factors are analyzed by WTC, which represent the frequency bands where the coherence between ET_o and these factors is significant (i.e., at the 95 % confidence level) across multiple time-frequency space. The frequencies are calculated based on time series data by decomposing the time series into different time scales and frequencies using wavelet transform. Subsequently, the coherence is calculated to identify which frequency bands exhibit significant coherence relationships.

2.3.3. Multiple wavelet coherence (MWC)

The WTC can only assess correlation coefficient in time-frequency domain between two time-series. However, MWC method can extend from two variables to multiple (> 2), providing an effective method to explore the synergistic effect of multiple driving factors. For a dependent variable Y and multiple factor variables X (≥ 2), the MWC at scale s and position u, $\rho_m^2(s,u)$, can be determined as (Hu and Si, 2016; Su et al., 2019)

$$\rho_m^2\left(s,u\right) = \overleftrightarrow{W}^{Y,X}\left(s,u\right)\frac{\overleftrightarrow{W}^{X,X-1}\left(s,u\right)\overleftrightarrow{W}^{Y,X}\left(s,u\right)^*}{\overleftrightarrow{W}^{Y,Y}\left(s,u\right)} \quad (14)$$

where $\overleftrightarrow{W}^{Y,X}(s,u)$ is the smoothed cross-wavelet power spectrum matrix between the Y and X; $\overleftrightarrow{W}^{X,X}(s,u)$ is the smoothed self-wavelet and cross-wavelet power spectrum matrix among X; $\overleftrightarrow{W}^{Y,Y}(s,u)$ is the smoothed wavelet power spectrum of Y; * is the complex conjugate (Hu and Si, 2016; Su et al., 2019).

2.3.4. Data analysis

For WTC and MWC, we adopted Monte Carlo method to calculate the wavelet coherence at the 95 % confidence level for each scale (Grinsted et al., 2004; Hu and Si, 2016). We calculated percentage area of significant coherence (PASC) within the entire wavelet time-frequency domain (Hu and Si, 2016), and mean values of significant WTC and MWC across varying time-frequency domains (WTC_{sig} and MWC_{sig}). The maximum PASC is the highest value of the percentage of the region where the coherence is significant (i.e. where ET_o and one or more variables are most closely linked) across multiple time-frequency space. This value indicates the extent to which the coherence between ET_o and one or more variables is strongest within a particular frequency band. The sub-maximum PASC value is the second-highest localized PASC value, trailing only the maximum value among all regions of significant coherence. It also demonstrates strong coherence between ET_o and the variable within a specific frequency band, albeit slightly less intense than the band corresponding to the maximum value. Calculating the maximum PASC assists in identifying which variables are most crucial in ET_o changes over time and understanding the strength of their coherence with ET_o, thereby facilitating further analysis of their influence mechanisms on ET_o changes. Additionally, calculating the sub-maximum PASC holds non-negligible value. In the MWC, if there are significant regions of coherence between ET_o and multiple variables, the maximum and sub-maximum PASC values may correspond to different variable combinations. This insight helps us identify which combinations of variables predominantly influence the variation of ET_o across multiple time-frequency spaces in subsequent studies.

A greater value of WTC_{sig} (or MWC_{sig}) combined with a larger value of PASC show more variation of ET_o explained by this or multiple meteorological variables. Generally, the WTC_{sig} (or MWC_{sig}) increases as the numbers of predictor variables increased, but this is not true for all the cases for PASC (Hu and Si, 2016). An increased PASC shows a significant increment in the ET_o variations explained by these predictor variables at the 95 % confidence level.

3. Results

3.1. Temporal patterns of ET_o

The CWT showed that ET_o and all meteorological variables (R_s, T_a, VPD, and u_2), except for u_2, exhibited similar fluctuation patterns across various temporal scales for almost all sites. Hence, here we presented power spectra of CWT for ET_o and R_s, T_a, VPD, and u_2 for one site as an example, as shown in Fig. 2. The power spectra for ET_o as well as all affecting factors exhibited frequency ranging from 2 days to 211 months, and a distinct spectral peak (excluding u_2) of ~374 days (1 year). This suggests a clearly annual scale in the ET_o variations and the associated meteorological factors, except for u_2. For u_2, 37.8 % of all stations showed an annual scale (~374 days), whereas remaining 375 stations showed main scale beyond the decade, and annual sub-scale.

3.2. Individual factor controlling the variability of ET_o

The relationships between ET_o and individual meteorological factors across multiple time-frequency domains at 653 meteorological stations in China using the WTC are shown in Figs. 1, 3, 4. Fig. 4a shows spatial distribution of the factor with the highest WTC_{sig} at each site, and values of WTC_{sig} between ET_o and each factor are shown in Fig. 1. Results showed that the WTC_{sig} for each site ranged from 0.78 to 0.95, and the highest WTC_{sig} among the four factors at each site exceeded 0.87. These results showed that there was a great co-variability between ET_o and the individual meteorological factor at each site. In addition, the dominant factor influencing ET_o across multiple time-frequency domains was R_s in 48.5 % of all sites (mainly in V and VI zones), followed by VPD in 47.6 % of all sites (mainly in II-IV zones), while was T_a (20 sites) and u_2 (5 sites) for limited stations (Fig. 4a). This is quite different from the daily scale, where daily ET_o was primary driven by daily R_n in 361 site, daily VPD in 286 sites and daily T_a in 6 sites based on Pearson-correlation analysis.

The spatial distribution of maximum and sub-maximum PASC values for meteorological factors is shown in Fig. 4b-c, and detailed spatial distribution of PASC values for each factor is shown in Fig. 3. The maximum values of PASC at each site ranged from 45.8 % to 97.8 % (mean = 78.9 %), and sub-maximum PASC was 27.8 %-91.9 % (mean = 62.6 %). The maximum and sub-maximum values of PASC were observed in 66.3 % (mainly in I-IV and VII zones) and 33.7 % of all sites, respectively, for VPD, and in 32.0 % (mainly in V and VI zones) and

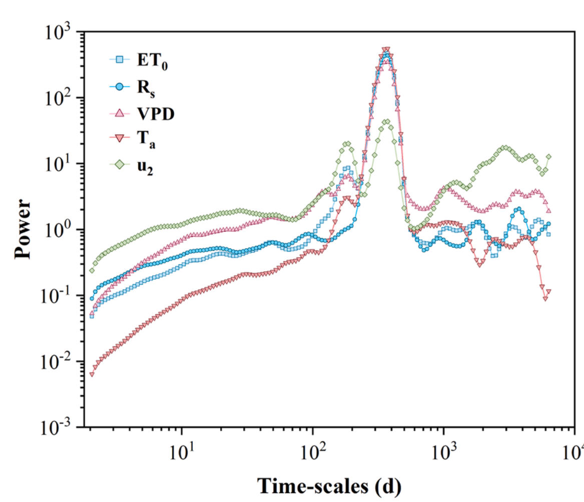

Fig. 2. Morlet wavelet power spectra of reference evapotranspiration (ET_o), solar radiation (R_s), vapor pressure deficit (VPD), air temperature (T_a), and wind speed at 2.0 m height (u_2) at Mohe, China (ID 50136).

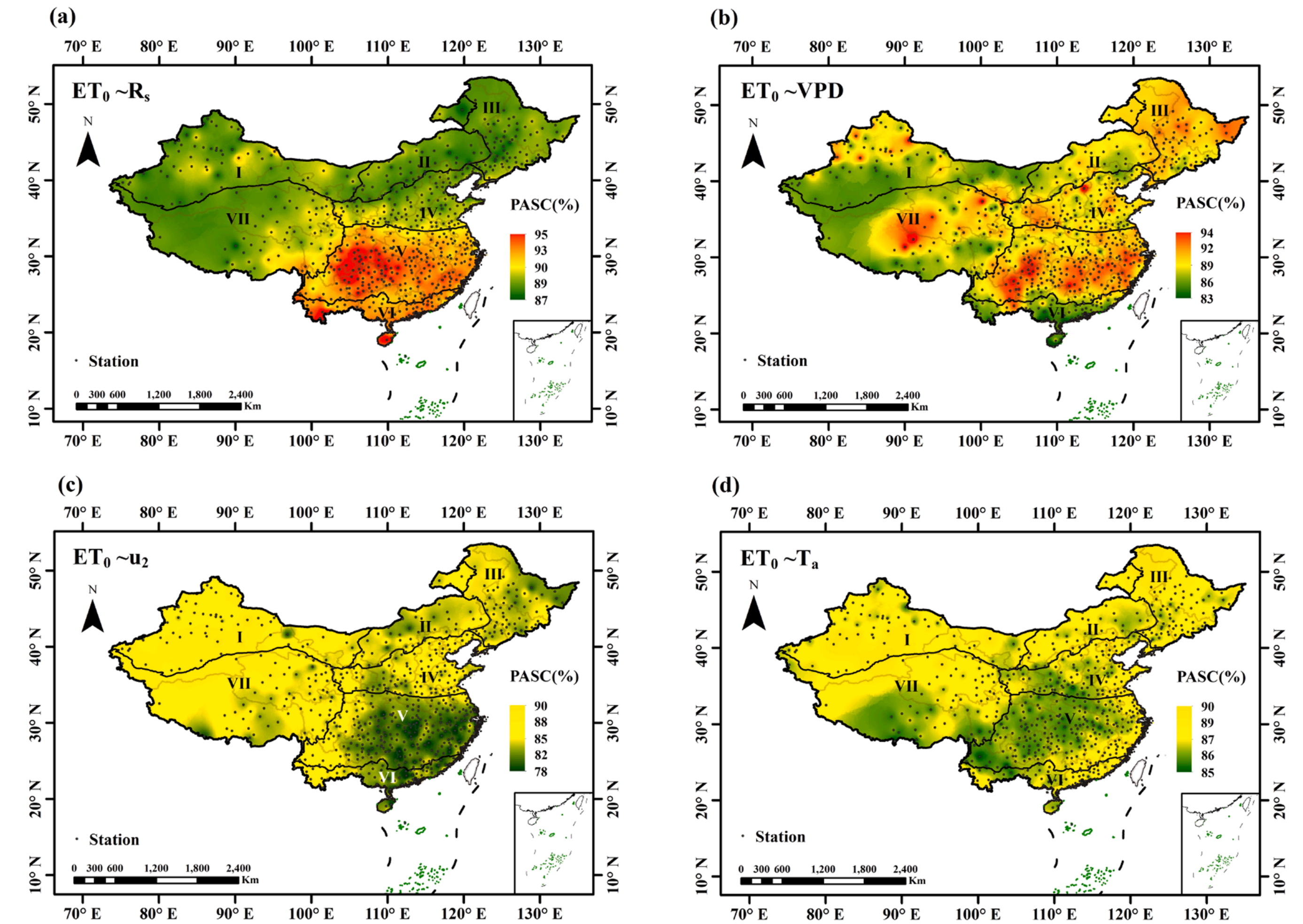

Fig. 3. Spatial distribution of percentage area of significant coherence (PASC) values between the reference evapotranspiration (ET_o) and solar radiation (R_s; a), vapor pressure deficit (VPD; b), wind speed at 2.0 m height (u_2; c), and air temperature (T_a; d) across time-frequency domain. I-VII regions are the same as in Fig. 1.

58.2 % of all sites, respectively, for R_s. Differently, these maximum and sub-maximum values were only observed in 11 (mainly in I zone) and 28 sites, respectively, for u_2 and in 0 and 25 sites, respectively, for T_a. These results suggest that on a national scale, VPD or R_s is the primary single factor driving variations in ET_o across time-frequency domain in majority sites, while u_2 is dominant in only a few sites.

The single meteorological factor that best explains variations of ET_o (i.e. highest PASC) in varying time-frequency domains are different. Therefore, we randomly chosen three stations to represent for each single meteorological factor with the highest PASC, as shown in Fig. 5. There was significant annual co-variance throughout the entire temporal period, consistent with the results of CWT analysis. The phase angles at an annual scale also showed that ET_o led VPD and T_a (negative phase angles) in most regions of China except in Yunnan and Tibet, while lagged behind R_s (positive phase angles) in most regions of China (Fig. 6). The regions where ET_o changes precede VPD and T_a the most located in the southern part of the Middle and Lower Yangtze River Basin (phase angle of ~160°; ~5.5 months) and Yunnan (phase angle of ~60°; ~2 months), respectively. Conversely, the regions where ET_o changes lag R_s the most located in the lower reaches of the Lancang River (phase angle of ~45°; ~1.5 months).

3.3. Two factors controlling the variability of ET_o

Exploring the impact of individual factors on ET_o can enhance identification of the primary factors. However, the variability of ET_o across time-frequency domain are affected by multiple factors. Hence, two factors having maximum and sub-maximum PASC were combined to evaluate whether they can further enhance the interpretation of ET_o variations across the multiple time-frequency domain. Among all two-factor combinations, the dominant is the VPD and R_s combination (90.2 % of all sites), encompassing all regions of China, except for most of Northwest China and a small portion of North China, which is dominant by combinations of VPD and u_2, as well as VPD and T_a (Fig. 7b). The MWC_{sig} of two-factor combinations in 653 sites ranged from 0.94 to 0.98 (mean = 0.96), which are greater than the corresponding highest WTC_{sig} among four factors by 3.3 %-10.6 % (mean = 0.90) (Fig. 7a). However, the PASC for two predictor variables ($PASC_{MWC}$) are not always greater than the highest PASC for one variable ($PASC_{WTC}$) (Fig. 7c), which will be detailed explained in the discussion part. Compared to $PASC_{WTC}$, the absolute values of $PASC_{MWC}$ increased in 78.4 % of all sites (specifically by 5 % in 40.7 % of all sites mainly distributed in I, IV, V, and VI zones), whereas decreased in 141 sites (primarily in II and III zones), indicating that considering more than one variable did not contribute to the explanation of ET_o variations across the time-frequency domains in these 141 sites (Fig. 7c).

Among all two-factor combinations (ET_o-VPD-R_s, ET_o-VPD-u_2, ET_o-VPD-T_a), when combinations including u_2 (mainly in VII zone), the absolute increment of $PASC_{MWC}$ over $PASC_{WTC}$ was at least 17 % and can reach up to 40 %. In contrast, the values of $PASC_{MWC}$ of ET_o-VPD-T_a (mainly in I and II zones) reduced compared to $PASC_{WTC}$ of ET_o-VPD for almost all sites (except for two sites on the Tibetan Plateau), suggesting a declined explanation of the ET_o series across the multiple time-frequency domains. Similarly, reduced values of $PASC_{MWC}$ for ET_o-

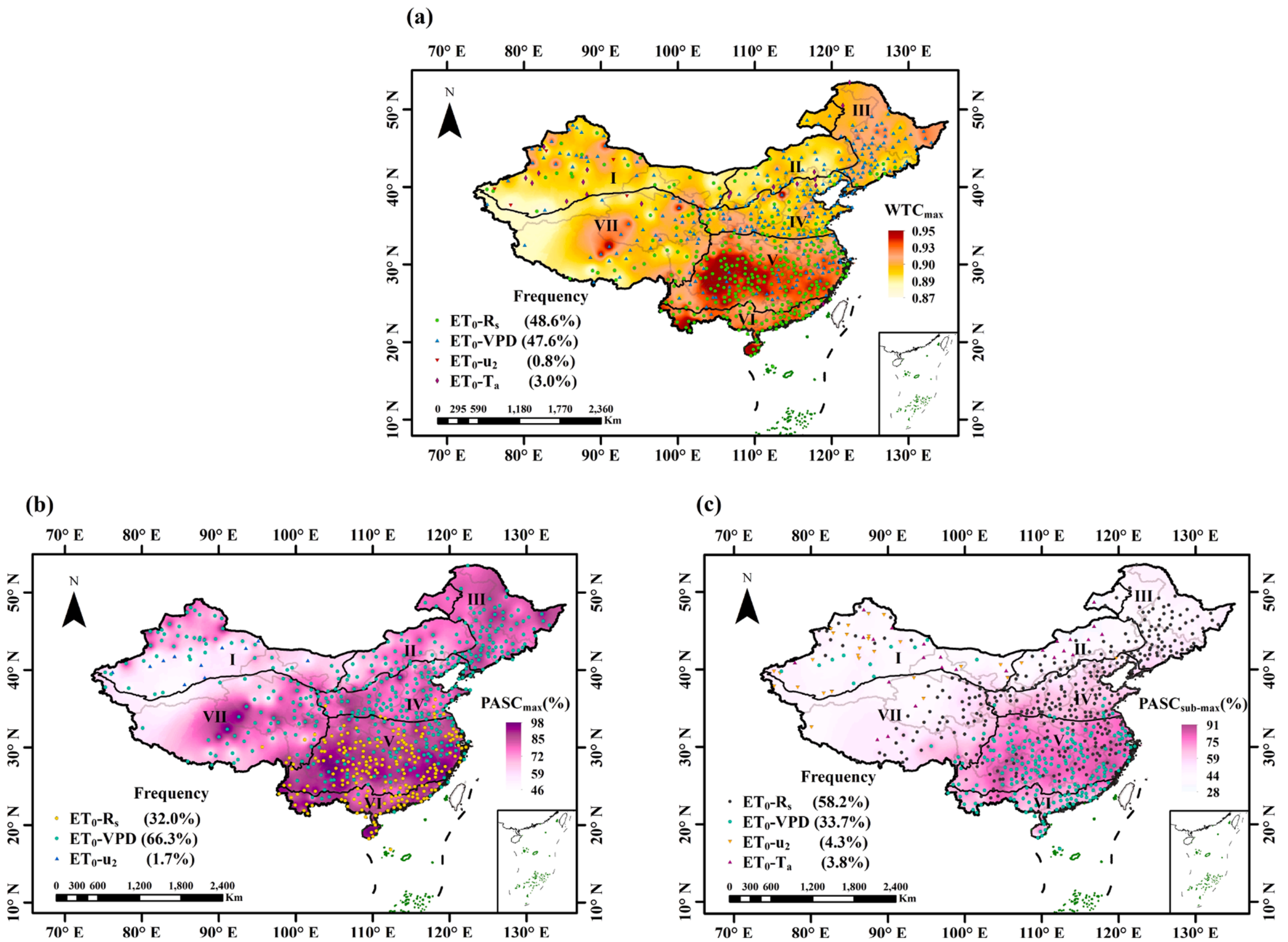

Fig. 4. Spatial distribution of maximum mean values of significant wavelet coherence across varying time-frequency domains (a), and maximum (b) and sub-maximum (c) percentage area of significant coherence (PASC) between reference evapotranspiration (ET$_o$) and solar radiation (R$_s$), vapor pressure deficit (VPD), air temperature (T$_a$), and wind speed at 2.0 m height (u_2). I-VII regions are the same as in Fig. 1.

VPD-R$_s$ or ET$_o$-R$_s$-VPD were also observed in some sites (mainly in I-III zones).

4. Discussion

4.1. Temporal patterns and dominant factors

Traditional time-series-based feature importance analysis methods, such as SHAP values (Li et al., 2024) and machine learning algorithms (Hao et al., 2015), provide a quantitative assessment of the overall contribution of individual variables. However, they are limited in capturing the dynamic coupling mechanisms of driving factors across the time-frequency domain (Guo et al., 2022). To more accurately assess the variation characteristics of ET$_o$ and its impact on agricultural water management, it is essential to analyze its key meteorological drivers across multiple time-frequency scales (Yao et al., 2020). This approach not only captures the periodic variations of meteorological factors but also reveals their dynamic influences on ET$_o$ across different temporal scales. Such an analysis enhances our understanding of the mechanisms underlying ET$_o$ variability and provides a robust foundation for developing more accurate predictive models.

In this study, we employed wavelet coherence analysis to reveal the multi-scale, time-varying characteristics of meteorological drivers of ET$_o$ across China and found that variability of ET$_o$, R$_s$, T$_a$, and VPD showed continuous annual periodicity for almost all sites using CWT. Similar patterns were also observed in the streamflow of many large rivers (Su et al., 2019) and PM2.5 concentration (Chen et al., 2020). This is not surprising since R$_s$, T$_a$, and VPD are evidently influenced by annual cycles, as observed in many regions (Chang et al., 2017), such as in the Horqin Sandy Land of China (Li et al., 2022). However, the primary time scale of u_2 extends beyond a decade at 375 stations, since u_2 spectrum is more complex than that of other factors (Chang et al., 2017). This complexity is mainly because u_2 is comprehensively affected by topography, underlying surface, atmospheric circulation (Cai et al., 2023), local climate conditions (Esau et al., 2012), and atmosphere pressure gradient (Wu et al., 2018). Therefore, in areas near the ocean or continental boundaries, u_2 is easily affected by local wind fields, resulting in pronounced interdecadal oscillations. In contrast, at inland stations far from the ocean, the annual oscillation of u_2 may be more pronounced due to local terrestrial effects or topographic factors (Shen et al., 2021).

Interestingly, VPD is the primary single factor controlling variations in ET$_o$ across the time-frequency space in 66.3 % of all sites in China, followed by R$_s$ (32.0 %) as indicated by highest PASC (Fig. 4b). However, this dominance varies with specific time scales. For example, at the seasonal scale, the contribution of R$_s$ to ET$_o$ changes is only 19.7 % in China, while RH contributes 14.3 % (Wang et al., 2017). At the annual scale, R$_s$ is the most important variable influencing ET$_o$ changes in China (Gao et al., 2017; She et al., 2017) and California (Ahmadi et al., 2022). This nonstationary characteristic suggests that attribution analyses conducted at a single temporal resolution may underestimate the

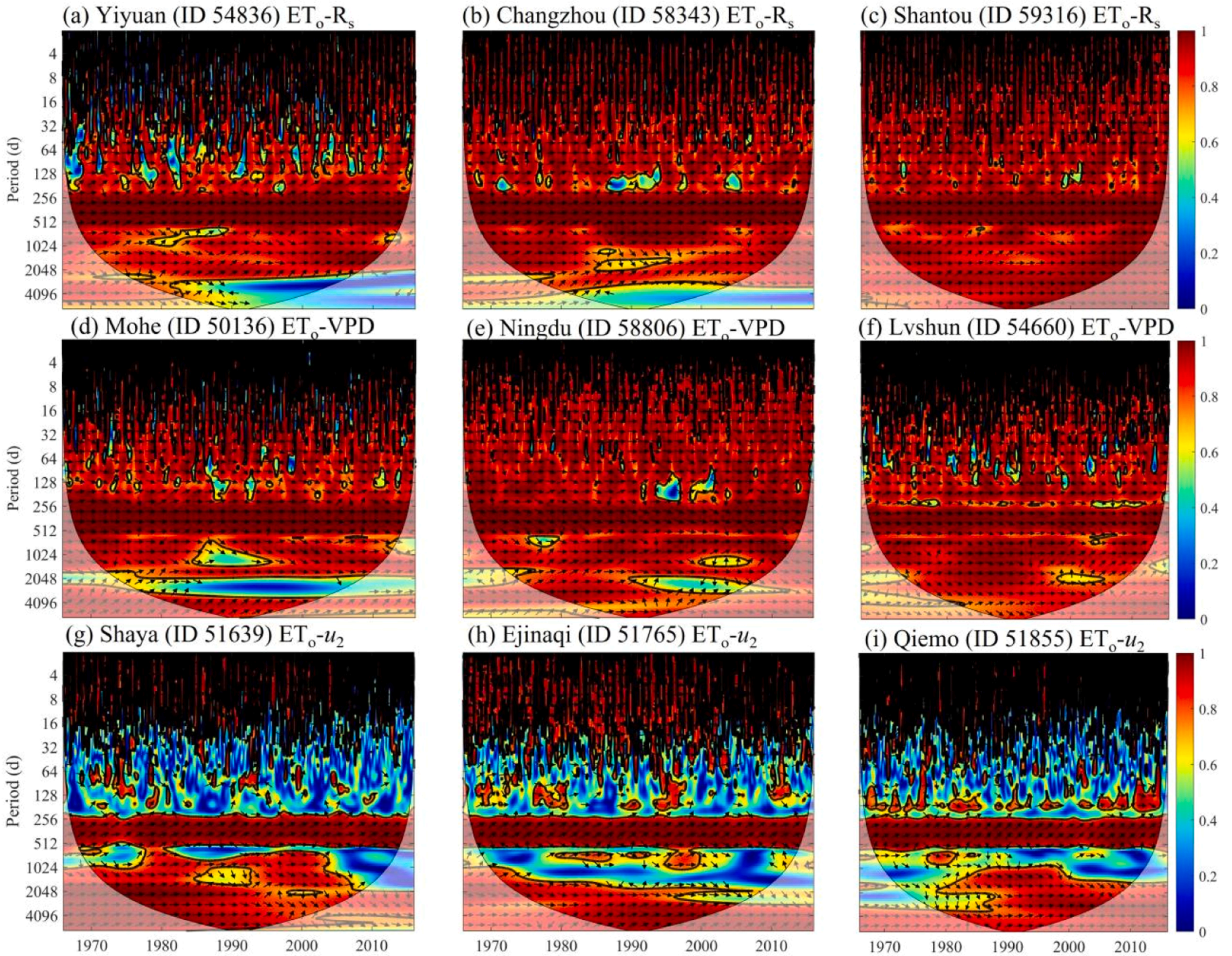

Fig. 5. The WTC results for the reference evapotranspiration (ET$_o$) and single meteorological factor (solar radiation (R$_s$; a-c), vapor pressure deficit (VPD; d-f), and wind speed at 2.0 m height (u_2; g-i)) that best explains (i.e. having highest PASC) variations of ET$_o$ in varying time-frequency domains in random selected sites. The climate zone for each station are as follows: 54836 (IV), 58343 (V), 59316 (VI), 50136 (III), 58806 (V), 54660 (IV), 51639 (I), 51756 (I), 51855 (I). I-VII regions are the same as in Fig. 1.

influence of key factors during specific periods (Kavetski et al., 2011). Annual-scale data are often sparse, which may result in insufficient statistical power to accurately assess the influence of individual features in feature importance analysis (Huang et al., 2018). At the seasonal scale, certain features may be closely linked to seasonal factors, making it more challenging to disentangle their effects (Noskov et al., 2024). Daily-scale data typically offer higher resolution and larger sample sizes, but this increased data volume also necessitates handling extensive computational tasks (Oubeidillah et al., 2014), thereby adding complexity and elevating computational costs in the analysis. In contrast, time-frequency domain approaches, by capturing multi-scale interactions, offer a more refined and physically interpretable perspective for understanding the dynamics of ET$_o$ (Koirala et al., 2010).

It is noteworthy that u_2 is dominant factor influencing ET$_o$ changes across the time-frequency domain in 11 sites. Wang et al. (2017) showed that u_2 is the primary factor at the seasonal scale in China. Gao et al. (2017) emphasized the importance of u_2 to ET$_o$ changes, indicating that u_2 is the sub-dominant factor affecting seasonal ET$_o$ changes. Valipour and Sefidkouhi (2018) highlighted that the threefold increase of u_2 after 2000 made it the most important variable influencing annual ET$_o$ changes in Iran. Collectively, these studies have elucidated the significant role of u_2 in driving ET$_o$ changes.

4.2. Regional disparities and causal analysis

From a regional perspective, the maximum PASC for R$_s$ (yellow dots in Fig. 4b) showed a relatively dense distribution in V and VI zones, indicting that R$_s$ is the primary influencing factor in these areas. This is mainly because these zones are located in the hot and humid regions of southern China, where the significant variability of R$_s$ results in its contribution being higher than that of other factors (Ahmadi et al., 2022). Other studies have pointed out that in the humid subtropical and tropical regions of China, R$_s$ is the most important controlling factor for ET$_o$ (Fan and Thomas, 2013; Liu et al., 2024; Yin et al., 2010). Similar results have been confirmed in the Poyang Lake (Ye et al., 2014) and the Sichuan Basin (Feng et al., 2014) where R$_s$ has been observed to significantly influence ET$_o$.

The maximum PASC for VPD (green dots in Fig. 4b) are mainly distributed in III, IV, V zones, and the central part of VII zone, suggesting that VPD is the main influencing factor for ET$_o$ in these areas. These climatic zones are widely distributed and mainly concentrated in North and South China, with some regions concentrated in Northeast China and the central Tibetan Plateau. Dong et al. (2024) indicated that VPD shows a significant upward trend in the temperate regions of northern China. Additionally, due to the influence of Asian continental humidity

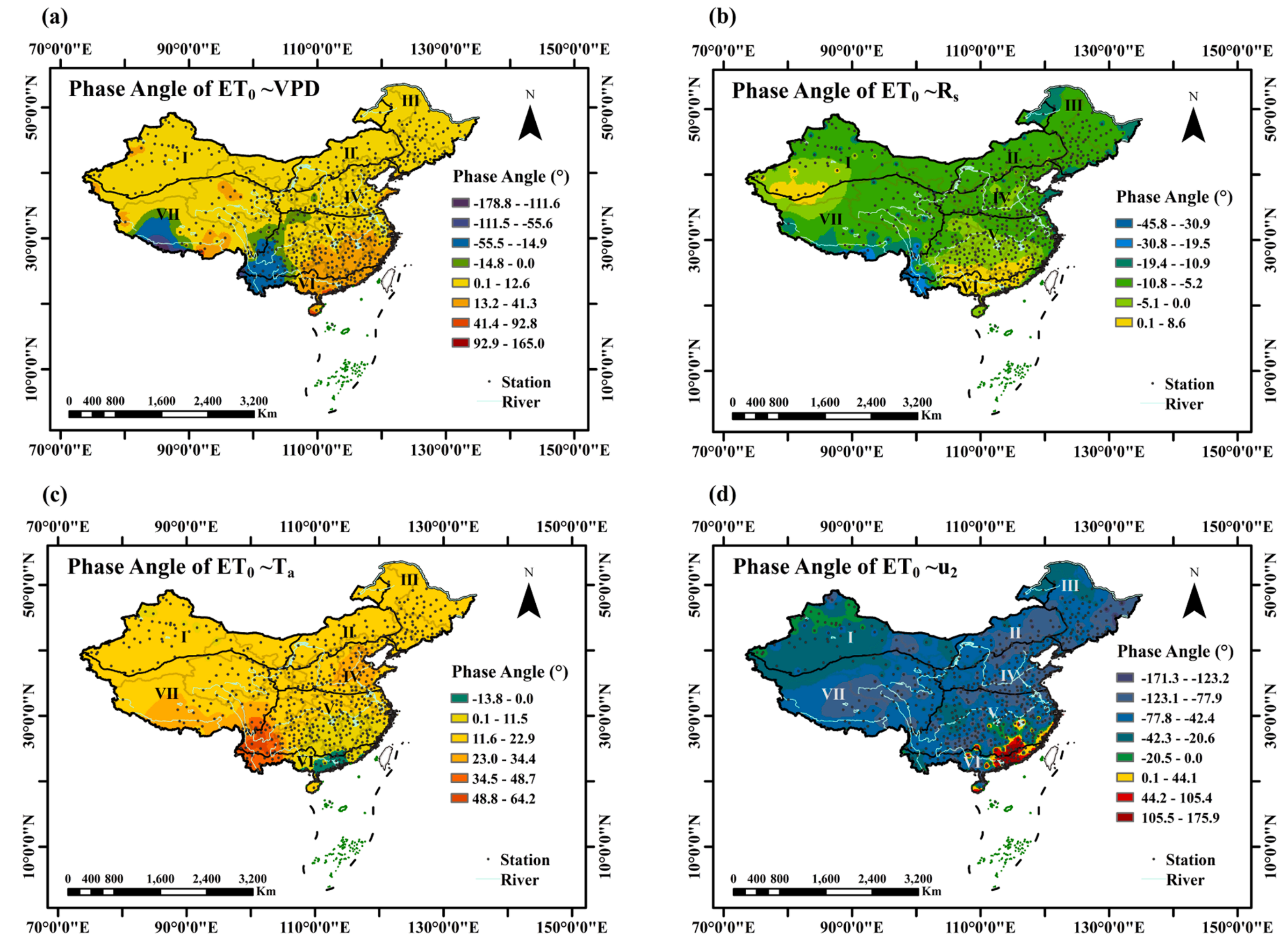

Fig. 6. Spatial distribution of phase angle between reference evapotranspiration (ET_o) and vapor pressure deficit (VPD; a), solar radiation (R_s; b), air temperature (T_a; c), and wind speed at 2.0 m height (u_2; d) at period of 374 d. I-VII regions are the same as in Fig. 1.

(Li et al., 2022), dry soil conditions (Deng et al., 2019), and freeze-thaw cycles (Chang et al., 2024), the variation of VPD in these regions is significant, making VPD more influential on ET_o compared to other factors. This may also be related to terrain, as the sensitivity of VPD to ET_o is higher in plains and mountainous areas than in coastal regions (Zhao et al., 2014).

The increase of VPD in tropical and temperate climates are more likely to result in positive ET_o changes than northern climates (Massmann et al., 2019). Li et al. (2021) indicated that the contribution of VPD to ET_o is significantly enhanced when temperature exceeds 15℃. These studies all confirm the strong coherence between VPD and ET_o in V zone (South China). Notably, this result does not contradict the high coherence of R_s and ET_o in different sites within V zone. Because different regions, even under the same climate conditions, may have different dominant factors, and the effects of climate change on ET_o can sometimes be contradictory (Pour et al., 2020).

Regions where u_2 has a significant effect on ET_o are mainly located in I and VII zones (Northwest Plateau region). Numerous studies have confirmed the strong influence of u_2 on ET_o changes in these areas (Ge et al., 2021; Li et al., 2014; Zheng and Wang, 2014). This is because the surface roughness of arid underlying surface is increased by irrigated agriculture, leading to a significant decrease in u_2 (Fu et al., 2022; Liu et al., 2024). The decreases of u_2 offset the upward effect caused by elevated T_a, which significantly contributes to the decline in ET_o (Wang et al., 2013). However, overall, the variability of ET_o is rarely dominated by u_2. This can be attributed to the fact that u_2 primarily affects water vapour transport and the controlling of the boundary layer conductance (McVicar et al., 2012; Tong et al., 2022).

Another result pointed out that the phase angles of VPD and T_a with ET_o are greater than 0 at the majority of sites, indicating that ET_o changes lag behind those of VPD and T_a. This is likely because when ET_o is fully decoupled from environmental factors, it reaches equilibrium with environmental conditions and becomes synchronized with changes in R_s, no longer being controlled by VPD. Therefore, when aerodynamic conductance is greater than 0, the lag between R_s and VPD results in a corresponding lag between ET_o and VPD (Zhang et al., 2014).

4.3. Synergistic efficacy of two factor combinations

Increasing the number of factor variables increased the MWC_{sig}, but not for $PASC_{MWC}$, due to the simultaneous increase in the statistical significance threshold (Hu and Si, 2016; Ng and Chan, 2012). This reduction in $PASC_{MWC}$ mainly occurred when there was strong collinearity between the additional and the existing variables (Hu et al., 2017; Vásquez et al., 2022). Such collinearity reduces the explanation of variations for response variables since the effect of additional factors in any specific time-frequency domain may have been included by the existing factors (Hu and Si, 2016).

In this study, greater (17 %-40 %) increment of $PASC_{MWC}$ over $PASC_{WTC}$ when combinations including u_2 was mainly contributed to less collinearity between u_2 and other factors, such as VPD. Additionally, u_2 is easily affected by complex terrain structures (Wang et al., 2022a),

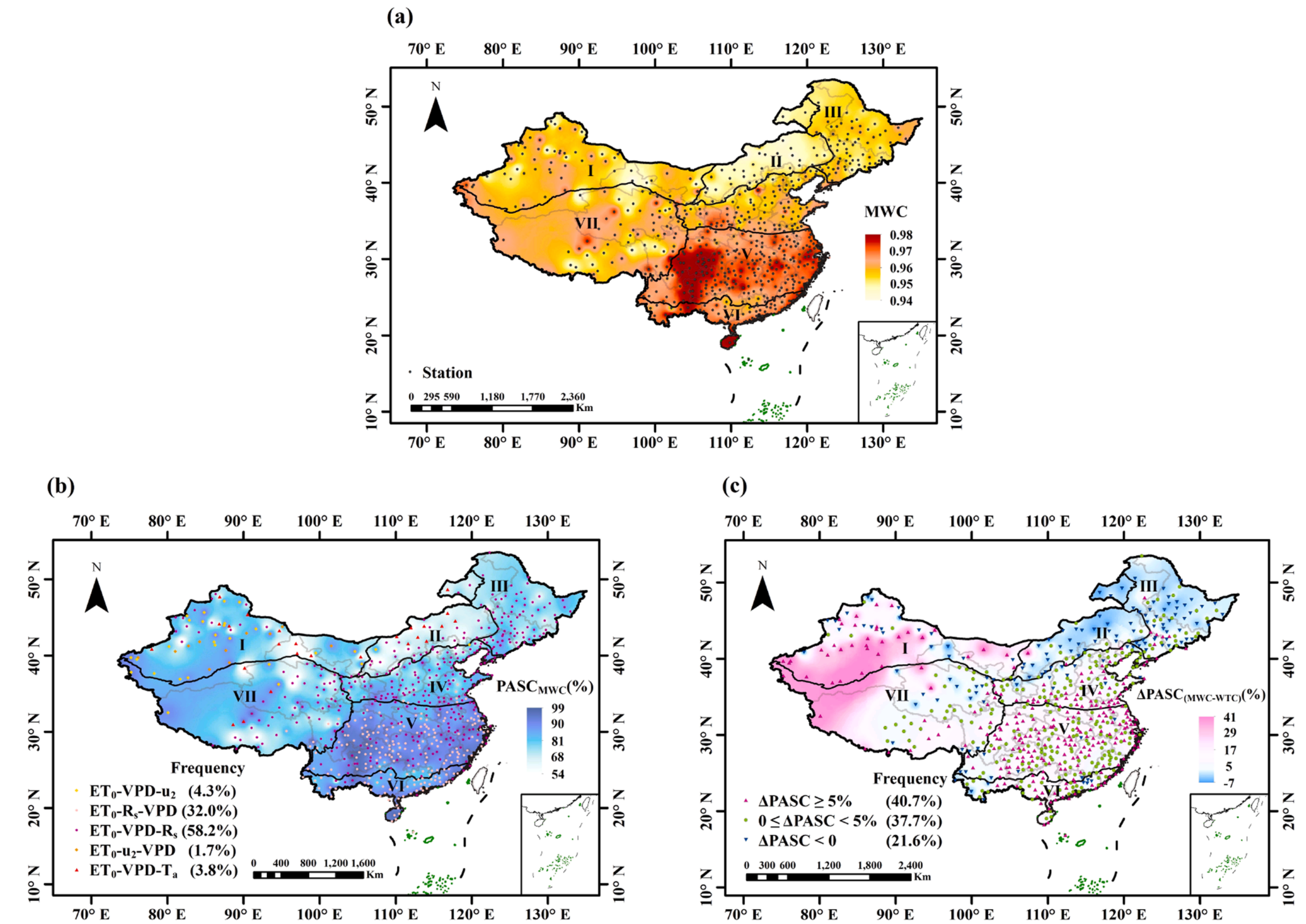

Fig. 7. Spatial distribution of maximum mean values of significant two-factor multiple wavelet coherence (MWC) across varying time-frequency domains (a), percentage area of significant coherence (PASC) values of MWC (b), and differences between PASC of MWC and maximum PASC of WTC (PASC$_{(MWC-WTC)}$) (c). I-VII regions are the same as in Fig. 1.

which may significantly influence wind flow and distribution by altering the wind speed profile, resulting in significantly local changes in u_2 (Wang et al., 2022b), thus greatly affects ET$_o$. McVicar et al. (2012) reviewed the recent slowdown in global near-surface winds and emphasized that one of its obvious effects is to partially offset any evaporation increase at high altitudes. Their study showed that land static force is a universal global phenomenon, emphasizing the contribution of u_2 to ET$_o$.

By the contrast, there are strong correlations between T$_a$ and VPD, as VPD is a composite factor of T$_a$ and RH, leading to a reduced PASC$_{MWC}$ for ET$_o$-VPD-T$_a$. In addition, relative strong collinearity between R$_s$ and VPD in some sites leads to either a reduction or a small increment (< 5 %) in PASC$_{MWC}$ for ET$_o$-VPD-R$_s$ (Fig. 7c). For practice, an additional significant factor in MWC should result in a PASC$_{MWC}$ increment greater than 5 % (Hu et al., 2017). This indicates that in 59.3 % of all sites, one variable (VPD or R$_s$) is sufficient to explain the variation of ET$_o$ across time-frequency domains (Fig. 7c).

5. Conclusions

Using wavelet analysis at 653 meteorological stations in China, we identified temporal patterns between ET$_o$ and each factor with CWT and analyzed the coherence of single and two factors with ET$_o$. The study showed that the ET$_o$, T$_a$, R$_s$, and VPD all exhibited annual periodicity, with a significant spectral peak at 1 year, reflecting the dominant influence of seasonal climate variability on these variables. In contrast, only 37.8 % of all sites showed an annual periodicity for u_2, while 62.2 % exhibited periodicities exceeding ten years. This highlights the complexity and regional variability of u_2 dynamics. Additionally, we found significant disparities in the coherence between ET$_o$ and meteorological factors across China. The PASC results revealed that VPD had the highest PASC value in 433 sites (66.3 %), while R$_s$ dominated at 209 stations (32 %). But u_2 was the dominant factor at only 11 stations (1.7 %). This suggests that VPD and R$_s$ are the primary drivers of ET$_o$ changes. Phase angle analyses indicated that, in most regions of China (excluding Yunnan and Tibet), the ET$_o$ changes lag behind VPD and T$_a$, but led R$_s$ across the multiple time-frequency domain. This suggests that the influence of different climatic factors on ET$_o$ varies temporally across regions, revealing the dynamic relationship between ET$_o$ and meteorological drivers. The MWC results showed that the response of ET$_o$ changes varies across different sites. At 59.3 % of all sites, ET$_o$ changes are more easily influenced by a single factor, which is sufficient to explain ET$_o$ changes. However, at 40.7 % of all sites, the combination of two factors (VPD-R$_s$ and VPD-u_2) significantly enhance the coherence with ET$_o$. This indicates that interactions between factors can amplify or attenuate their effects on ET$_o$ variability, showing the diversity and complexity of ET$_o$ driving mechanisms across different regions. This study provides novel insights into understanding the variations of ET$_o$ across multiple time-frequency domains.

CRediT authorship contribution statement

Zhang Tao: Writing – review & editing, Validation. **Luo Yufeng:** Writing – review & editing, Validation. **Hu Wei:** Writing – review & editing, Validation, Methodology. **Zhao Shuting:** Writing – review & editing, Writing – original draft, Validation. **Wu Jinglong:** Writing – review & editing, Writing – original draft, Visualization, Validation. **Qiu Rangjian:** Writing – review & editing, Supervision, Software, Methodology, Investigation, Funding acquisition, Formal analysis, Conceptualization.

Declaration of Competing Interest

The authors declare that they have no known competing financial interests or personal relationships that could have appeared to influence the work reported in this paper.

Acknowledgments

We acknowledge support from the National Natural Science Foundation of China (52322904, 52179036).

Data availability

Data will be made available on request.

References

Ahmadi, A., Daccache, A., Snyder, R.L., Suvočarev, K., 2022. Meteorological driving forces of reference evapotranspiration and their trends in California. Sci. Total Environ. 849, 157823. https://doi.org/10.1016/j.scitotenv.2022.157823.

Allen, R., Pereira, L., Raes, D., Smith, M., Allen, R.G., Pereira, L.S., Martin, S., 1998. Crop evapotranspiration: guidelines for computing crop water requirements, FAO irrigation and drainage paper 56. FAO 56.

Araghi, A., Baygi, M.M., Adamowski, J., Malard, J., Nalley, D., Hasheminia, S.M., 2015. Using wavelet transforms to estimate surface temperature trends and dominant periodicities in Iran based on gridded reanalysis data. Atmos. Res. 155, 52–72. https://doi.org/10.1016/j.atmosres.2014.11.016.

Cai, Z., You, Q., Chen, H.W., Zhang, R., Zuo, Z., Dai, G., Chen, D., Cohen, J., Zolina, O., Gulev, S.K., 2023. Interdecadal variability of the warm Arctic-cold Eurasia pattern linked to the Barents oscillation. Atmos. Res. 287, 106712. https://doi.org/10.1016/j.atmosres.2023.106712.

Cazelles, B., Chavez, M., Berteaux, D., Ménard, F., Vik, J.O., Jenouvrier, S., Stenseth, N. C., 2008. Wavelet analysis of ecological time series. Oecologia 156 (2), 287–304. https://doi.org/10.1007/s00442-008-0993-2.

Chang, T., Liu, F., Ko, H., Huang, M., 2017. Oscillation characteristic study of wind speed, global solar radiation and air temperature using wavelet analysis. Appl. Energy 190, 650–657. https://doi.org/10.1016/j.apenergy.2016.12.149.

Chang, Y., Ding, Y., Zhang, S., Shangguan, D., Qin, J., Zhao, Q., 2024. Contribution of climatic variables and their interactions to reference evapotranspiration changes considering freeze-thaw cycles in the Tibetan Plateau during 1960-2022. Atmos. Res. 305, 107425. https://doi.org/10.1016/j.atmosres.2024.107425.

Chen, X., Yin, L., Fan, Y., Song, L., Ji, T., Liu, Y., Tian, J., Zheng, W., 2020. Temporal evolution characteristics of PM2.5 concentration based on continuous wavelet transform. Sci. Total Environ. 699, 134244. https://doi.org/10.1016/j.scitotenv.2019.134244.

Chong, K.L., Lai, S.H., El-Shafie, A., 2019. Wavelet transform based method for river stream flow time series frequency analysis and assessment in tropical environment. Water Resour. Manag. 33 (6), 2015–2032. https://doi.org/10.1007/s11269-019-02226-7.

Chou, C., 2011. Wavelet-based multi-scale entropy analysis of complex rainfall time series. Entropy 13 (1), 241–253. https://doi.org/10.3390/e13010241.

Citakoglu, H., Cobaner, M., Haktanir, T., Kisi, O., 2014. Estimation of monthly mean reference evapotranspiration in Turkey. Water Resour. Manag. 28 (1), 99–113. https://doi.org/10.1007/s11269-013-0474-1.

CMA Meteorological Data Centre, 2019. ⟨https://data.cma.cn/⟩ (accessed 6 February 2019).

Deng, C., Zhang, B., Cheng, L., Hu, L., Chen, F., 2019. Vegetation dynamics and their effects on surface water-energy balance over the Three-North Region of China. Agric. For. Meteorol. 275, 79–90. https://doi.org/10.1016/j.agrformet.2019.05.012.

Ding, R., Kang, S., Vargas, R., Zhang, Y., Hao, X., 2013. Multiscale spectral analysis of temporal variability in evapotranspiration over irrigated cropland in an arid region. Agric. Water Manag. 130, 79–89. https://doi.org/10.1016/j.agwat.2013.08.019.

Ding, X., Li, Q., Lin, L., He, Q., Shao, Y., 2019. Fast time-frequency manifold learning and its reconstruction for transient feature extraction in rotating machinery fault diagnosis. Measurement 141, 380–395. https://doi.org/10.1016/j.measurement.2019.04.030.

Dong, J., Wu, L., Zeng, W., Xiao, X., He, J., 2024. Analysis of spatial-temporal trends and causes of vapor pressure deficit in China from 1961 to 2020. Atmos. Res. 299, 107199. https://doi.org/10.1016/j.atmosres.2023.107199.

Esau, I., Luhunga, P., Djolov, G., Rautenbach, C.J.D.W., Zilitinkevich, S., 2012. Links between observed micro-meteorological variability and land-use patterns in the highveld priority area of South Africa. Meteorol. Atmos. Phys. 118 (3-4), 129–142. https://doi.org/10.1007/s00703-012-0218-4.

Fan, J., Yue, W., Wu, L., Zhang, F., Cai, H., Wang, X., Lu, X., Xiang, Y., 2018. Evaluation of SVM, ELM and four tree-based ensemble models for predicting daily reference evapotranspiration using limited meteorological data in different climates of China. Agric. For. Meteorol. 263, 225–241. https://doi.org/10.1016/j.agrformet.2018.08.019.

Fan, Z., Thomas, A., 2013. Spatiotemporal variability of reference evapotranspiration and its contributing climatic factors in Yunnan Province, SW China, 1961-2004. Clim. Change 116 (2), 309–325. https://doi.org/10.1007/s10584-012-0479-4.

Feng, Y., Cui, N., Wei, X., Zhao, L., Wang, J., 2014. Temporal-spatial distribution characteristics and causes analysis of reference crop evapotranspiration in hilly area of central Sichuan. Trans. Chin. Soc. Agric. Eng. 30 (14), 78–86. https://doi.org/10.3969/j.issn.1002-6819.2014.14.011.

Feng, Z., Liang, M., Chu, F., 2013. Recent advances in time-frequency analysis methods for machinery fault diagnosis: a review with application examples. Mech. Syst. Signal Proc. 38 (1), 165–205. https://doi.org/10.1016/j.ymssp.2013.01.017.

Fu, J., Kang, S., Zhang, L., Li, X., Gentine, P., Niu, J., 2022. Amplified warming induced by large-scale application of water-saving techniques. Environ. Res. Lett. 17 (3), 034018. https://doi.org/10.1088/1748-9326/ac4b52.

Gao, Z., He, J., Dong, K., Li, X., 2017. Trends in reference evapotranspiration and their causative factors in the West Liao River basin, China. Agric. For. Meteorol. 232, 106–117. https://doi.org/10.1016/j.agrformet.2016.08.006.

Ge, J., Feng, D., You, Q., Zhang, W., Zhang, Y., 2021. Characteristics and causes of surface wind speed variations in Northwest China from 1979 to 2019. Atmos. Res. 254, 105527. https://doi.org/10.1016/j.atmosres.2021.105527.

Gedalof, Z., Peterson, D.L., Mantua, N.J., 2004. Columbia river flow and drought since 1750. J. Am. Water Resour. Assoc. 40 (6), 1579–1592. https://doi.org/10.1111/j.1752-1688.2004.tb01607.x.

Ghaemi, A., Rezaie-Balf, M., Adamowski, J., Kisi, O., Quilty, J., 2019. On the applicability of maximum overlap discrete wavelet transform integrated with MARS and M5 model tree for monthly pan evaporation prediction. Agric. For. Meteorol. 278, 107647. https://doi.org/10.1016/j.agrformet.2019.

Gocić, M., Motamedi, S., Shamshirband, S., Petković, D., Sudheer, C., Hashim, R., Arif, M., 2015. Soft computing approaches for forecasting reference evapotranspiration. Comput. Electron. Agric. 113, 164–173. https://doi.org/10.1016/j.compag.2015.02.010.

Grinsted, A., Moore, J.C., Jevrejeva, S., 2004. Application of the cross wavelet transform and wavelet coherence to geophysical time series. Nonlinear Process Geophys 11 (5-6), 561–566. https://doi.org/10.5194/npg-11-561-2004.

Guo, J., Sun, H., Du, B., 2022. Multivariable time series forecasting for urban water demand based on temporal convolutional network combining random forest feature selection and discrete wavelet transform. Water Resour. Manag. 36 (9), 3385–3400. https://doi.org/10.1007/s11269-022-03207-z.

Han, J., Wang, J., Zhao, Y., Wang, Q., Zhang, B., Li, H., Zhai, J., 2018. Spatio-temporal variation of potential evapotranspiration and climatic drivers in the Jing-Jin-Ji region, North China. Agric. For. Meteorol. 256, 75–83. https://doi.org/10.1016/j.agrformet.2018.03.002.

Hao, P., Zhan, Y., Wang, L., Niu, Z., Shakir, M., 2015. Feature selection of time series modis data for early crop classification using random forest: a case study in Kansas, USA. Remote Sens 7 (5), 5347–5369. https://doi.org/10.3390/rs70505347.

Hu, W., Si, B., 2021. Technical Note: Improved partial wavelet coherency for understanding scale-specific and localized bivariate relationships in geosciences. Hydrol. Earth Syst. Sci. 25 (1), 321–331. https://doi.org/10.5194/hess-25-321-2021.

Hu, W., Si, B.C., 2016. Technical note: Multiple wavelet coherence for untangling scale-specific and localized multivariate relationships in geosciences. Hydrol. Earth Syst. Sci. 20 (8), 3183–3191. https://doi.org/10.5194/hess-20-3183-2016.

Hu, W., Si, B.C., Biswas, A., Chau, H.W., 2017. Temporally stable patterns but seasonal dependent controls of soil water content: evidence from wavelet analyses. Hydrol. Process. 31 (21), 3697–3707. https://doi.org/10.1002/hyp.11289.

Hu, X., Chen, M., Liu, D., Li, D., Jin, L., Liu, S., Cui, Y., Dong, B., Khan, S., Luo, Y., 2021. Reference evapotranspiration change in Heilongjiang Province, China from 1951 to 2018: The role of climate change and rice area expansion. Agric. Water Manag. 253, 106912. https://doi.org/10.1016/j.agwat.2021.106912.

Huang, Z., Hejazi, M., Li, X., Tang, Q., Vernon, C., Leng, G., Liu, Y., Döll, P., Eisner, S., Gerten, D., 2018. Reconstruction of global gridded monthly sectoral water withdrawals for 1971–2010 and analysis of their spatiotemporal patterns. Hydrol. Earth Syst. Sci. 22 (4), 2117–2133. https://doi.org/10.5194/hess-22-2117-2018.

Jerin, J.N., Islam, H.M.T., Islam, A.R.M.T., Shahid, S., Hu, Z., Badhan, M.A., Chu, R., Elbeltagi, A., 2021. Spatiotemporal trends in reference evapotranspiration and its driving factors in Bangladesh. Theor. Appl. Climatol. 144 (1-2), 793–808. https://doi.org/10.1007/s00704-021-03566-4.

Joshi, N., Gupta, D., Suryavanshi, S., Adamowski, J., Madramootoo, C.A., 2016. Analysis of trends and dominant periodicities in drought variables in India: A wavelet transform based approach. Atmos. Res. 182 (dec.), 200–220. https://doi.org/10.1016/j.atmosres.2016.07.030.

Kang, Y., Chen, P., Cheng, X., Zhang, S., Song, S., 2022. Novel hybrid machine learning framework with decomposition-transformation and identification of key modes for estimating reference evapotranspiration. Agric. Water Manag. 273, 107882. https://doi.org/10.1016/j.agwat.2022.107882.

Kavetski, D., Fenicia, F., Clark, M.P., 2011. Impact of temporal data resolution on parameter inference and model identification in conceptual hydrological modeling: insights from an experimental catchment. W05501 Water Resour. Res. 47 (5). https://doi.org/10.1029/2010WR009525.

Khanmohammadi, N., Rezaie, H., Montaseri, M., Behmanesh, J., 2017. The effect of different meteorological parameters on the temporal variations of reference evapotranspiration. Environ. Earth Sci. 76 (15), 13. https://doi.org/10.1007/s12665-017-6871-7.

Kim, J., Wang, X., Kang, C., Yu, J., Li, P., 2021. Forecasting air pollutant concentration using a novel spatiotemporal deep learning model based on clustering, feature selection and empirical wavelet transform. Sci. Total Environ. 801, 149654. https://doi.org/10.1016/j.scitotenv.2021.149654.

Koirala, S.R., Gentry, R.W., Mulholland, P.J., Perfect, E., Schwartz, J.S., 2010. Time and frequency domain analyses of high-frequency hydrologic and chloride data in an east Tennessee watershed. J. Hydrol. 387 (3-4), 256–264. https://doi.org/10.1016/j.jhydrol.2010.04.014.

Li, C., Wu, P.T., Li, X.L., Zhou, T.W., Sun, S.K., Wang, Y.B., Luan, X.B., Yu, X., 2017. Spatial and temporal evolution of climatic factors and its impacts on potential evapotranspiration in Loess Plateau of Northern Shaanxi, China. Sci. Total Environ. 589, 165–172. https://doi.org/10.1016/j.scitotenv.2017.02.122.

Li, Q., Ji, Y., Zhu, M., Zhu, X., Sun, L., 2024. Unsupervised feature selection using chronological fitting with Shapley Additive explanation (SHAP) for industrial time-series anomaly detection. Appl. Soft Comput. 155, 111426. https://doi.org/10.1016/j.asoc.2024.111426.

Li, S., Wang, G., Sun, S., Hagan, D.F.T., Chen, T., Dolman, H., Liu, Y., 2021. Long-term changes in evapotranspiration over China and attribution to climatic drivers during 1980-2010. J. Hydrol. 595, 126037. https://doi.org/10.1016/j.jhydrol.2021.126037.

Li, X., Zhang, S., Liu, T., Lin, X., Li, R., Wang, S., 2022. Time scale and influencing factor variations of water and heat fluxes in sandy land. Hydrol. Res. 53 (7), 983–1000. https://doi.org/10.2166/nh.2022.020.

Li, Z., Zheng, F., Liu, W., 2012. Spatiotemporal characteristics of reference evapotranspiration during 1961-2009 and its projected changes during 2011-2099 on the Loess Plateau of China. Agric. For. Meteorol. 154, 147–155. https://doi.org/10.1016/j.agrformet.2011.10.019.

Li, Z., Chen, Y., Yang, J., Wang, Y., 2014. Potential evapotranspiration and its attribution over the past 50years in the arid region of Northwest China. Hydrol. Process. 28 (3), 1025–1031. https://doi.org/10.1002/hyp.9643.

Liang, L., Li, L., Liu, Q., 2010. Temporal variation of reference evapotranspiration during 1961-2005 in the Taoer River basin of Northeast China. Agric. For. Meteorol. 150 (2), 298–306. https://doi.org/10.1016/j.agrformet.2009.11.014.

Liu, W., Zhang, B., Wei, Z., Wang, Y., Tong, L., Guo, J., Han, X., Han, C., 2024. Heterogeneity analysis of main driving factors affecting potential evapotranspiration changes across different climate regions. Sci. Total Environ. 912, 168991. https://doi.org/10.1016/j.scitotenv.2023.168991.

Luo, Z., Xiao, Q., 2014. Time-frequency features of signal analysis and its application in mechanical fault diagnosis. Adv. Mater. Res. 834, 1065–1068. https://doi.org/10.4028/www.scientific.net/AMR.834-836.1065.

Mahmoud, S.H., Gan, T.Y., 2020. Multidecadal variability in the Nile River basin hydroclimate controlled by ENSO and Indian Ocean dipole. Sci. Total Environ. 748, 141529. https://doi.org/10.1016/j.scitotenv.2020.141529.

Maraun, D., Kurths, J., 2004. Cross wavelet analysis: significance testing and pitfalls. Nonlinear Process Geophys. 11 (4), 505–514. https://doi.org/10.5194/npg-11-505-2004.

Martínez, B., Gilabert, M.A., 2009. Vegetation dynamics from NDVI time series analysis using the wavelet transform. Remote Sens. Environ. 113 (9), 1823–1842. https://doi.org/10.1016/j.rse.2009.04.016.

Massmann, A., Gentine, P., Lin, C., 2019. When does vapor pressure deficit drive or reduce evapotranspiration. J. Adv. Model. Earth Syst. 11 (10), 3305–3320. https://doi.org/10.1029/2019MS001790.

McVicar, T.R., Roderick, M.L., Donohue, R.J., Li, L.T., Van Niel, T.G., Thomas, A., Grieser, J., Jhajharia, D., Himri, Y., Mahowald, N.M., Mescherskaya, A.V., Kruger, A. C., Rehman, S., Dinpashoh, Y., 2012. Global review and synthesis of trends in observed terrestrial near-surface wind speeds: Implications for evaporation. J. Hydrol. 416, 182–205. https://doi.org/10.1016/j.jhydrol.2011.10.024.

Ng, E.K.W., Chan, J.C.L., 2012. Interannual variations of tropical cyclone activity over the north Indian Ocean. Int. J. Climatol. 32 (6), 819–830. https://doi.org/10.1002/joc.2304.

Noskov, Y.A., Manasypov, R.M., Ermolaeva, N.I., Antonets, D.V., Shirokova, L.S., Pokrovsky, O.S., 2024. Environmental factors controlling seasonal and spatial variability of zooplankton in thermokarst lakes along a permafrost gradient of Western Siberia. Sci. Total Environ. 922, 171284. https://doi.org/10.1016/j.scitotenv.2024.171284.

Nourani, V., Ghasemzade, M., Mehr, A.D., Sharghi, E., 2019. Investigating the effect of hydroclimatological variables on Urmia Lake water level using wavelet coherence measure. J. Water Clim. Chang. 10 (1), 13–29. https://doi.org/10.2166/wcc.2018.261.

Oubeidillah, A.A., Kao, S., Ashfaq, M., Naz, B.S., Tootle, G., 2014. A large-scale, high-resolution hydrological model parameter data set for climate change impact assessment for the conterminous US. Hydrol. Earth Syst. Sci. 18 (1), 67–84. https://doi.org/10.5194/hess-18-67-2014.

Paredes, P., Pereira, L.S., 2019. Computing FAO56 reference grass evapotranspiration PM-ETo from temperature with focus on solar radiation. Agric. Water Manag. 215, 86–102. https://doi.org/10.1016/j.agwat.2018.12.014.

Paredes, P., Trigo, I., de Bruin, H., Simões, N., Pereira, L.S., 2021. Daily grass reference evapotranspiration with Meteosat Second Generation shortwave radiation and reference ET products. Agric. Water Manag. 248, 106543. https://doi.org/10.1016/j.agwat.2020.106543.

Pereira, A.R., Pruitt, W.O., 2004. Adaptation of the Thornthwaite scheme for estimating daily reference evapotranspiration. Agric. Water Manag. 66 (3), 251–257. https://doi.org/10.1016/j.agwat.2003.11.003.

Pereira, L.S., Allen, R.G., Smith, M., Raes, D., 2015. Crop evapotranspiration estimation with FAO56: Past and future. Agric. Water Manag. 147, 4–20. https://doi.org/10.1016/j.agwat.2014.07.031.

Pereira, L.S., Paredes, P., Hunsaker, D.J., -Urrea, R., Jovanovic, N., 2021. Updates and advances to the FAO56 crop water requirements method. Agric. Water Manag. 248, 106697. https://doi.org/10.1016/j.agwat.2020.106697.

Pour, S.H., Wahab, A.K.A., Shahid, S., Ismail, Z.B., 2020. Changes in reference evapotranspiration and its driving factors in peninsular Malaysia. Atmos. Res. 246, 105096. https://doi.org/10.1016/j.atmosres.2020.105096.

Qiu, R., Du, T., Kang, S., Chen, R., Wu, L., 2015. Assessing the SIMDualKc model for estimating evapotranspiration of hot pepper grown in a solar greenhouse in Northwest China. Agric. Syst. 138, 1–9. https://doi.org/10.1016/j.agsy.2015.05.001.

Qiu, R., Liu, C., Cui, N., Wu, Y., Wang, Z., Li, G., 2019. Evapotranspiration estimation using a modified Priestley-Taylor model in a rice-wheat rotation system. Agric. Water Manag. 224, 105755. https://doi.org/10.1016/j.agwat.2019.105755.

Qiu, R., Li, L., Liu, C., Wang, Z., Zhang, B., Liu, Z., 2022. Evapotranspiration estimation using a modified crop coefficient model in a rotated rice-winter wheat system. Agric. Water Manag. 264, 107501. https://doi.org/10.1016/j.agwat.2022.107501.

Qiu, R., Katul, G.G., Zhang, L., Qin, S., Jiang, X., 2025. The effects of changing environments, abiotic stresses, and management practices on cropland evapotranspiration: A review. Rev. Geophys. 63 (1), e2024RG000858. https://doi.org/10.1029/2024RG000858.

Rallo, G., Paço, T.A., Paredes, P., Puig-Sirera, À., Massai, R., Provenzano, G., Pereira, L. S., 2021. Updated single and dual crop coefficients for tree and vine fruit crops. Agric. Water Manag. 250, 106645. https://doi.org/10.1016/j.agwat.2020.106645.

Rhif, M., Abbes, A.B., Farah, I.R., Martínez, B., Sang, Y., 2019. Wavelet transform application for/in non-stationary time-series analysis: A review. Appl. Sci. -Basel 9 (7), 1345. https://doi.org/10.3390/app9071345.

Sang, Y., 2013. A review on the applications of wavelet transform in hydrology time series analysis. Atmos. Res. 122, 8–15. https://doi.org/10.1016/j.atmosres.2012.11.003.

She, D., Xia, J., Zhang, Y., 2017. Changes in reference evapotranspiration and its driving factors in the middle reaches of Yellow River Basin, China. Sci. Total Environ. 607, 1151–1162. https://doi.org/10.1016/j.scitotenv.2017.07.007.

Shen, L., Zhao, C., Yang, X., 2021. Insight into the seasonal variations of the sea-land breeze in Los Angeles with respect to the effects of solar radiation and climate type. J. Geophys. Res. -Atmos. 126 (6), e2020JD033197. https://doi.org/10.1029/2020JD033197.

Shi, Z., Xu, L., Yang, X., Guo, H., Dong, L., Song, A., Zhang, X., Shan, N., 2017. Trends in reference evapotranspiration and its attribution over the past 50 years in the Loess Plateau, China: implications for ecological projects and agricultural production. Stoch. Environ. Res. Risk Assess. 31 (1), 257–273. https://doi.org/10.1007/s00477-015-1203-5.

Sreedevi, V., Adarsh, S., Nourani, V., 2022. Multiscale coherence analysis of reference evapotranspiration of north-western Iran using wavelet transform. J. Water Clim. Chang. 13 (2), 505–521. https://doi.org/10.2166/wcc.2021.379.

Su, L., Miao, C., Duan, Q., Lei, X., Li, H., 2019. Multiple-wavelet coherence of world's large rivers with meteorological factors and ocean signals. J. Geophys. Res. -Atmos. 124 (9), 4932–4954. https://doi.org/10.1029/2018JD029842.

Sun, C., Zheng, Z., Chen, W., Wang, Y., 2020. Spatial and temporal variations of potential evapotranspiration in the Loess Plateau of China during 1960-2017. Sustainability 12 (1), 354. https://doi.org/10.3390/su12010354.

Tang, Y., Tang, Q., 2021. Variations and influencing factors of potential evapotranspiration in large Siberian river basins during 1975-2014. J. Hydrol. 598, 126443. https://doi.org/10.1016/j.jhydrol.2021.126443.

Tao, L., Cui, Z., He, Y., Yang, D., 2024. An explainable multiscale LSTM model with wavelet transform and layer-wise relevance propagation for daily streamflow forecasting. Sci. Total Environ. 929, 172465. https://doi.org/10.1016/j.scitotenv.2024.172465.

Tie, Q., Hu, H., Tian, F., Holbrook, N.M., 2018. Comparing different methods for determining forest evapotranspiration and its components at multiple temporal scales. Sci. Total Environ. 633, 12–29. https://doi.org/10.1016/j.scitotenv.2018.03.082.

Tong, B., Guo, J., Xu, H., Wang, Y., Li, H., Bian, L., Zhang, J., Zhou, S., 2022. Effects of soil moisture, net radiation, and atmospheric vapor pressure deficit on surface evaporation fraction at a semi-arid grass site. Sci. Total Environ. 849, 157890. https://doi.org/10.1016/j.scitotenv.2022.157890.

Torrence, C., Compo, G.P., 1998. A practical guide to wavelet analysis. Bull. Am. Meteorol. Soc. 79 (1), 61–78. https://doi.org/10.1175/1520-0477(1998)079< 0061:APGTWA> 2.0.CO;2.

Valipour, M., Sefidkouhi, M.A.G., 2018. Temporal analysis of reference evapotranspiration to detect variation factors. Int. J. Glob. Warm. 14 (3), 385–401. https://doi.org/10.1504/IJGW.2018.090403.

Valipour, M., Sefidkouhi, M.A.G., Raeini-Sarjaz, M., 2017. Selecting the best model to estimate potential evapotranspiration with respect to climate change and magnitudes of extreme events. Agric. Water Manag. 180, 50–60. https://doi.org/10.1016/j.agwat.2016.08.025.

Vásquez, C., Célleri, R., Córdova, M., Carrillo-Rojas, G., 2022. Improving reference evapotranspiration (ETo) calculation under limited data conditions in the high

Tropical Andes. Agric. Water Manag. 262, 107439. https://doi.org/10.1016/j.agwat.2021.107439.
Wang, C., Chen, J., Gu, L., Wu, G., Tong, S., Xiong, L., Xu, C., 2023. A pathway analysis method for quantifying the contributions of precipitation and potential evapotranspiration anomalies to soil moisture drought. J. Hydrol. 621, 129570. https://doi.org/10.1016/j.jhydrol.2023.129570.
Wang, W., Xing, W., Shao, Q., Yu, Z., Peng, S., Yang, T., Yong, B., Taylor, J., Singh, V.P., 2013. Changes in reference evapotranspiration across the Tibetan Plateau: Observations and future projections based on statistical downscaling. J. Geophys. Res. -Atmos. 118 (10), 4049–4068. https://doi.org/10.1002/jgrd.50393.
Wang, Q., Luo, K., Wu, C., Mu, Y., Tan, J., Fan, J., 2022b. Diurnal impact of atmospheric stability on inter-farm wake and power generation efficiency at neighboring onshore wind farms in complex terrain. Energy Conv. Manag. 267, 115897. https://doi.org/10.1016/j.enconman.2022.115897.
Wang, Q., Luo, K., Wu, C., Zhu, Z., Fan, J., 2022a. Mesoscale simulations of a real onshore wind power base in complex terrain: Wind farm wake behavior and power production. Energy 241, 122873. https://doi.org/10.1016/j.energy.2021.122873.
Wang, Z., Xie, P., Lai, C., Chen, X., Wu, X., Zeng, Z., Li, J., 2017. Spatiotemporal variability of reference evapotranspiration and contributing climatic factors in China during 1961-2013. J. Hydrol. 544, 97–108. https://doi.org/10.1016/j.jhydrol.2016.11.021.
Wu, C., Zhang, X., Wang, W., Lu, C., Zhang, Y., Qin, W., Tick, G.R., Liu, B., Shu, L., 2021. Groundwater level modeling framework by combining the wavelet transform with a long short-term memory data-driven model. Sci. Total Environ. 783, 146948. https://doi.org/10.1016/j.scitotenv.2021.146948.
Wu, J., Zha, J., Zhao, D., Yang, Q., 2018. Changes of wind speed at different heights over eastern China during 1980-2011. Int. J. Climatol. 38 (12), 4476–4495. https://doi.org/10.1002/joc.5681.
Wu, Q., Tan, J., Guo, F., Li, H., Chen, S., 2019. Multi-scale relationship between land surface temperature and landscape pattern based on wavelet coherence: the case of metropolitan Beijing, China. Remote Sens 11 (24), 3021. https://doi.org/10.3390/rs11243021.
Wu, S., Yao, J., Wang, Y., Zhao, W., 2023. Influencing factors of PM2.5 concentration in the typical urban agglomerations in China based on wavelet perspective. Environ. Res. 237, 116641. https://doi.org/10.1016/j.envres.2023.116641.
Xiang, K., Li, Y., Horton, R., Feng, H., 2020. Similarity and difference of potential evapotranspiration and reference crop evapotranspiration - a review. Agric. Water Manag. 232, 106043. https://doi.org/10.1016/j.agwat.2020.106043.
Yang, Y., Chen, R., Song, Y., Han, C., Liu, J., Liu, Z., 2019. Sensitivity of potential evapotranspiration to meteorological factors and their elevational gradients in the Qilian Mountains, northwestern China. J. Hydrol. 568, 147–159. https://doi.org/10.1016/j.jhydrol.2018.10.069.
Yao, N., Li, Y., Lei, T., Peng, L., 2018. Drought evolution, severity and trends in mainland China over 1961-2013. Sci. Total Environ. 616, 73–89. https://doi.org/10.1016/j.scitotenv.2017.10.327.
Yao, N., Li, Y., Dong, Q., Li, L., Peng, L., Feng, H., 2020. Influence of the accuracy of reference crop evapotranspiration on drought monitoring using standardized precipitation evapotranspiration index in mainland China. Land Degrad. Dev. 31 (2), 266–282. https://doi.org/10.1002/ldr.3447.
Ye, X., Li, X., Liu, J., Xu, C., Zhang, Q., 2014. Variation of reference evapotranspiration and its contributing climatic factors in the Poyang Lake catchment, China. Hydrol. Process. 28 (25), 6151–6162. https://doi.org/10.1002/hyp.10117.
Yin, Y., Wu, S., Chen, G., Dai, E., 2010. Attribution analyses of potential evapotranspiration changes in China since the 1960s. Theor. Appl. Climatol. 101 (1-2), 19–28. https://doi.org/10.1007/s00704-009-0197-7.
Zarei, A.R., Mahmoudi, M.R., Shabani, A., 2021. Using the fuzzy clustering and principle component analysis for assessing the impact of potential evapotranspiration calculation method on the modified RDI index. Water Resour. Manag. 35 (11), 3679–3702. https://doi.org/10.1007/s11269-021-02910-7.
Zhang, Q., Manzoni, S., Katul, G., Porporato, A., Yang, D., 2014. The hysteretic evapotranspiration—Vapor pressure deficit relation. J. Geophys. Res. -Biogeosci. 119 (2), 125–140. https://doi.org/10.1002/2013JG002484.
Zhang, T., Qiu, R., Ding, R., Wu, J., Clothier, B., 2023. Multi-scale spectral characteristics of latent heat flux over flooded rice and winter wheat rotation system. Agric. Water Manag. 288, 108471. https://doi.org/10.1016/j.agwat.2023.108471.
Zhao, L., Xia, J., Sobkowiak, L., Li, Z., 2014. Climatic characteristics of reference evapotranspiration in the Hai River Basin and their attribution. Water 6 (6), 1482–1499. https://doi.org/10.3390/w6061482.
Zhao, L., Zhao, X., Pan, X., Shi, Y., Qiu, Z., Li, X., Xing, X., Bai, J., 2022. Prediction of daily reference crop evapotranspiration in different Chinese climate zones: Combined application of key meteorological factors and Elman algorithm. J. Hydrol. 610, 127822. https://doi.org/10.1016/j.jhydrol.2022.127822.
Zhao, S., Wu, L., Xiang, Y., Zhang, F., 2024. Forecasting short-term methane based on corrected numerical weather prediction outputs. J. Clean. Prod. 460, 142500. https://doi.org/10.1016/j.jclepro.2024.142500.
Zhao, X., Wilcox, M., Scherrer, H., 1983. The sporal sector transition regions in the interplanetary magnetic fields. Chin. J. Space Sci. 3 (1), 1–9. https://doi.org/10.11728/cjss1983.01.001.
Zheng, C., Wang, Q., 2014. Spatiotemporal variations of reference evapotranspiration in recent five decades in the arid land of Northwestern China. Hydrol. Process. 28 (25), 6124–6134. https://doi.org/10.1002/hyp.10109.
Zhou, S., Williams, A.P., Berg, A.M., Cook, B.I., Zhang, Y., Hagemann, S., Lorenz, R., Seneviratne, S.I., Gentine, P., 2019. Land-atmosphere feedbacks exacerbate concurrent soil drought and atmospheric aridity. Proc. Natl. Acad. Sci. U. S. A. 116 (38), 18848–18853. https://doi.org/10.1073/pnas.1904955116.
Zhou, Z., Liu, S., Ding, Y., Fu, Q., Wang, Y., Cai, H., Shi, H., 2022. Assessing the responses of vegetation to meteorological drought and its influencing factors with partial wavelet coherence analysis. J. Environ. Manag. 311, 114879. https://doi.org/10.1016/j.jenvman.2022.114879.